Cluster-luminescent polysiloxane nanomaterials: adjustable full-color ultralong room temperature phosphorescence and a highly sensitive response to silver ions†

Shuaiqi Wang,[a] Xiaolang Wang,[a] Shangwei Feng,[a] Wei Lv,[a] Meijuan Lin, [iD] [a] Qidan Ling [iD] [a] and Zhenghuan Lin [iD] *[a,b]

Non-conjugated cluster luminescent materials have attracted much attention because of their good bio-compatibility and low environmental toxicity. However, it has been difficult to achieve tunable cluster luminescent nanomaterials. Herein, a series of non-conjugated polysiloxane nanomaterials are synthesized from organosiloxane by a low temperature solution method. Polysiloxanes with terminal groups of amino (PAS) and urea (PUS) exhibit high luminescence quantum yield and long-lived room temperature phosphorescence (RTP) due to the formation of suitable spatial clusters. Interestingly, doping different types and contents of nonaromatic guest small molecules can effectively regulate the structure and composition of the clusters in polysiloxanes, thus resulting in full-color unconventional cluster luminescence with high quantum yield (up to 44%), long lifetime (up to 560 ms), and emission wavelengths from 380 nm to 753 nm. Additionally, the fluorescence and RTP of PAS are very sensitive to silver ions, which can be used to probe Ag⁺ in aqueous solutions with a detection limit as low as 0.027 nM. This double response detection can not only avoid the interference of background fluorescence, but also verify the accuracy of experimental results.

Introduction

Traditional luminescent materials are mainly aromatic compounds constructed by conjugated bonds.[1–3] Due to the presence of a large π system and rigid structure, they can achieve high luminescence efficiency and adjustable luminescent colors.[4–6] However, these aromatic luminescent materials have some disadvantages: low biocompatibility and high toxicity, especially the aggregation-caused quenching (ACQ) existing in some planar conjugated molecules. Some natural polymers, such as protein,[7] cellulose[8] and sodium alginate,[9] have certain self-luminescence or photoluminescence properties. However, the unclear luminescence mechanism has limited their development. Since the emergence of non-conjugated luminescent polyamidoamine (PAMAM),[10] polyethylene glycol (PEG),[11] and

polyurea (PU),[12] research studies on this kind of non-traditional luminescent material have made some progress. Generally, such non-conjugated materials contain many heteroatoms such as N, O and S.[13] When these heteroatoms are aggregated together, it is possible to produce photoluminescence (defined as "cluster luminescence") from space conjugation.[14–16]

The so-called "clusters" are aggregates formed in space by functional groups through some weak interactions. At present, cluster induced phosphorescence (CIP), even long-lived room temperature phosphorescence (RTP) or afterglow, have been realized through crystal engineering[17–20] and polymerization induction.[21] However, CIP efficiency is highly dependent on the morphology of the material, requiring high crystal quality (for small molecules)[22,23] or large molecular weight (for polymers).[24,25] Therefore, it is difficult to realize the CIP of amorphous nanomaterials which have huge application potential in biological imaging, optoelectronic devices, and information storage. It is necessary to develop a simple method to obtain nanomaterials with long lifetime CIP.

Silica is a common inorganic nanosphere. Its surface has enough defects to promote electron storage.[26] Meanwhile, silica nanospheres can also prevent, fix and protect light-emitting groups, resulting in high-efficiency and stable

[a]*Fujian Key Laboratory of Polymer Materials, College of Chemistry and Materials Science, Fujian Normal University, Fuzhou 350007, China.*
E-mail: zhlin@fjnu.edu.cn
[b]*Fujian Provincial Key Laboratory of Advanced Materials Oriented Chemical Engineering, Fuzhou, 350007, China*

†Electronic supplementary information (ESI) available: Experimental details and additional characterization and analysis. See DOI: https://doi.org/10.1039/d2qi00914e

This journal is © the Partner Organisations 2022

Inorg. Chem. Front., 2022, **9**, 3619–3626 | **3619**

emission.[27–29] However, the CIP of amorphous non-traditional luminescent nanomaterials has not been achieved. In view of the crucial role of terminal functional groups in the formation of clusters, in this work, a series of polysiloxane nanomaterials were synthesized by the low temperature solution method from siloxane precursors with the terminal groups of urea (US), vinyl (VS), chlorine (CS), amino (AS), and sulfhydryl (SS) (Fig. 1). Polysiloxane nanomaterials based on amino (PAS) and urea (PUS) achieved efficient blue light emission with a Φ up to 30%, and a blue-green afterglow with a lifetime of 120 ms. Then, to regulate the structure and composition of clusters, organic compounds containing carbonyl groups were doped into PAS. Interestingly, the full-color long afterglow with emission wavelengths ranging from 380 nm to 753 nm was realized, by changing the type and doping ratio of organic components. The luminescence quantum yield is up to 44% and the phosphorescence lifetime is up to 576 ms. Lastly, PAS was employed as a luminescent probe to recognize metal ions in aqueous solutions. It shows excellent response to Ag^+ with a detection limit of 0.027 nM, which is close to the minimum detection limit of the reported Ag^+ probes (Table S1†).[30]

Results and discussion

Synthesis and structure characterization

As shown in Scheme S1,† a siloxane monomer was firstly hydrolyzed in 0.1 mol L^{-1} HCl aqueous solution at room temperature, and then gelated and aged at 90 °C. After washing with deionized water and drying in a vacuum oven, polysiloxane nanomaterials were easily prepared under mild conditions in a yield more than 95%. By changing the types of siloxane monomers, a series of polysiloxanes (PAS, PUS, PSS, PCS and PVS) with different functional groups can be obtained. Powder X-ray diffraction (PXRD) results show that all obtained polysiloxanes are amorphous (Fig. 2a). There is only a wide diffraction peak at about 23°, which is the characteristic peak of SiO_2. Fig. 2b is the high-resolution scanning electron microscopy (HRSEM) image of PAS at 300 000 times magnification. The results show that the microstructure of PAS is irregular microspheres with an average particle size of about 23 nm, and that the accumulation of particles will form irregular interconnected pores. Due to some same functional
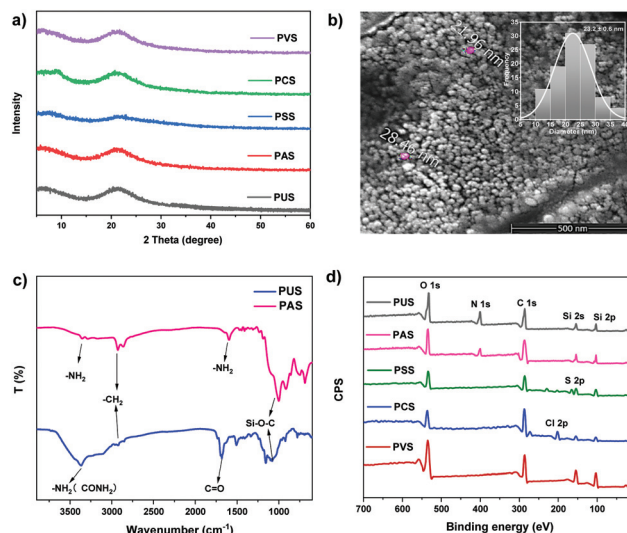

Fig. 2 (a) PXRD curves of polysiloxanes. (b) HRSEM photograph of PAS (insets: histograms of particle size distributions fitted to weighted Gaussian distributions). (c) IR spectra of PUS and PAS. (d) Full-scan XPS spectra of PUS, PAS, PSS, PCS and PVS.

groups, PAS and PUS show similar infrared (IR) spectra (Fig. 2c). However, in the IR spectrum of PUS, there is an obvious characteristic peak at 1680 cm^{-1}, which belongs to the stretching vibration of C=O in the amide group. The IR spectra of the other three materials are shown in Fig. S1.† The stretching vibration peak of C=C bonds in PVS appears at 1610 cm^{-1}. The characteristic peak of sulfhydryl groups in PSS is at 2550 cm^{-1}. The IR spectra of PSS and PCS show a strong signal at 3500–3600 cm^{-1}, because a large number of OH groups exist in the system.

The full-scan X-ray photoelectron spectroscopy (XPS) spectra of the five polysiloxane nanomaterials are shown in Fig. 2d. There are obvious characteristic peaks of C 1s, O 1s, Si 2s and Si 2p found for all polysiloxanes, indicating that they contain three elements of C, O and Si. In addition, the characteristic peaks of N 1s (for PAS and PUS), S 2p (for PSS), and Cl 2p (for PCS) are also found in the XPS spectra. Consequently, except for C, O and Si elements, both PAS and PUS have an N element, while PSS and PCS have S and Cl elements, respectively. PVS is only composed of C, O and Si, and there are no characteristic peaks of other elements. From the fine XPS spectrum of PUS (Fig. S2†), it is found that the C 1s spectrum exhibits three typical peaks at 284.8, 286.1 and 288.8 eV, corresponding to C–C, C–N and C=O groups, respectively. The N 1s spectrum shows C–N and C(O)–NH characteristic peaks at 399.9 eV and 403.1 eV, respectively. The binding energies of 532.4 eV and 535.4 eV in the O 1s spectrum can be assigned to O–Si and C=O, respectively. The peak at 103 eV in the Si 2p spectrum corresponds to SiO_2. The fine XPS spectra of the other polysiloxane nanomaterials are shown in Fig. S3–S6.† These characterization data confirm the structures of these polysiloxanes.
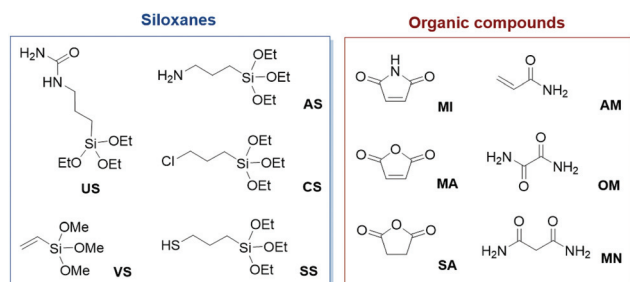

Fig. 1 Structures of inorganic and organic precursors of hybrid nanomaterials.

3620 | *Inorg. Chem. Front.*, 2022, **9**, 3619–3626

This journal is © the Partner Organisations 2022

Photophysical properties of polysiloxanes

All polysiloxanes emit blue light under a 365 nm of UV lamp (Fig. 3a). Their prompt emission spectra show that the emission wavelength ranges from 357 nm to 455 nm (Fig. 3b). The excitation spectra of these polysiloxanes except that of PVS are very broad (Fig. S7†). In particular, for PAS and PUS, their excitation spectra cover the range from 280 to 420 nm, which suggests that there are different luminescent centers in these materials. Interestingly, PAS and PUS exhibit blue-green and green afterglow, respectively, after turning off the UV lamp. The 1 ms delay emission spectra in Fig. 3c shows that the RTP emission is at 498 nm (for PAS) and 485 nm (for PUS). From the transient luminescence decay curves of PAS and PUS (Fig. 3d), their lifetime of RTP can be calculated to be around 120 ms. Compared with other polysiloxanes, PAS and PUS display higher luminescence quantum yield up to 30.2%, which indicates that NH_2-induced compact clusters with space conjugation are formed in the structures of PAS and PUS. Because the size of clusters is not uniform, the luminescence of PAS and PUS has excitation wavelength-dependent properties regardless of prompt emission (Fig. S8†) or delayed emission (Fig. 3e and f). It is worth noting that there is a long wavelength emission at 650 nm in the delay spectrum of PUS. In addition to amino groups, PUS has carbonyl groups; thus the emission at 650 nm is likely to be caused by newly formed clusters involving CO and NH_2 groups. Their detailed photophysical data are listed in Tables S2 and S3.†

Combined with the structural characteristics of PAS and PUS, a possible cluster model of the polysiloxanes is proposed, as shown in Fig. 4. The above morphology analysis shows that polysiloxane nanomaterials are composed of irregular nano-microspheres (Fig. 2b). Each small nanosphere is actually a three-dimensional crosslinked silica skeleton with a terminal amino or urea functional group. These terminal groups gather to form clusters with silica and uncrosslinked hydroxyl groups. PAS clusters are mainly formed by weak interactions, such as N–H⋯O and OH⋯N hydrogen bonding. Due to these weak forces, the clusters with rich lone pair electrons can be fixed to form a stable spatial conjugate system, which improves the rate of the ISC process and triplet exciton radiation transition, thus resulting in a long-lived blue RTP at 498 nm. The more
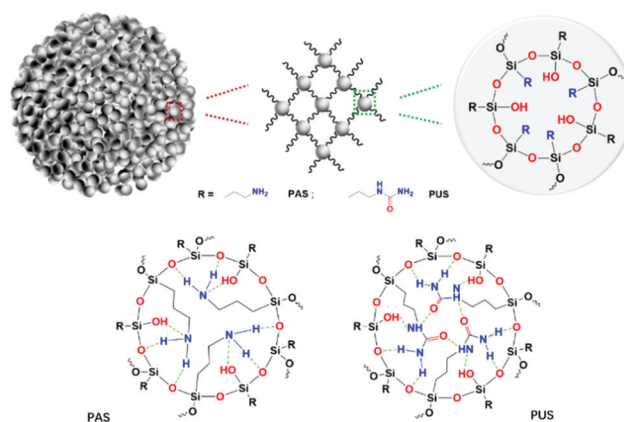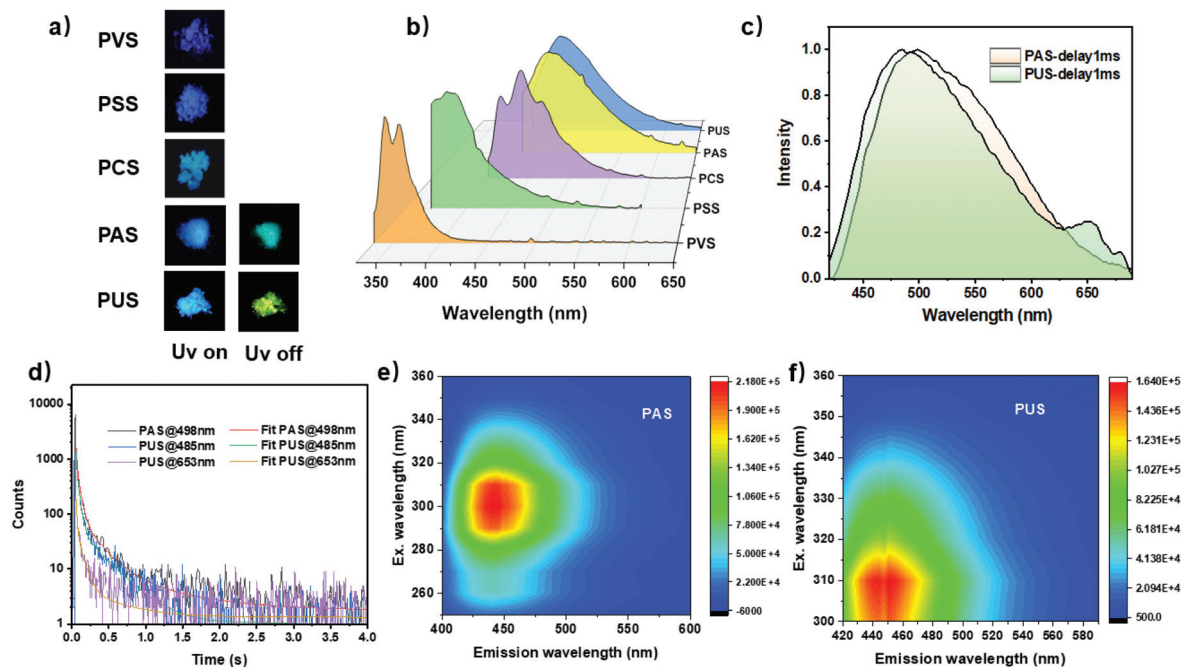

Fig. 4 Possible cluster model of PAS and PUS.

Fig. 3 (a) Photographs of polysiloxanes before and after UV light is turned off. (b) Photoluminescence spectra of polysiloxanes. (c) Delayed emission spectra of PAS and PUS (t_d = 1 ms). (d) Time-resolved luminescence decay profiles of PAS and PUS. Excitation−emission mappings of PAS (e) and PUS (f) with a 1 ms delay.

complex clusters can be formed in the skeleton of PUS compared to that in PAS. In addition to N–H···O and OH···N hydrogen bonds, there is also hydrogen-bonding between N–H and C=O. Therefore, the delayed emission spectrum of PUS has a new shoulder peak at 650 nm beside a wide main peak at 485 nm. Because the size of the clusters is uncontrollable, a variety of different luminescent centers can be generated, which is responsible for the excitation wavelength-dependent emission of PAS and PUS. Taking PAS as an example, several possible clusters with different sizes are proposed and shown in Fig. S9.† Thermogravimetric analysis plots of PAS and PUS show that they have high thermal stability with the 5% weight loss temperature of 210 °C and 228 °C, respectively (Fig. S10†).

Regulation of polysiloxane RTP

The structure and composition of clusters play an important role in the RTP performance of PAS and PUS. Therefore, changing the cluster structures will effectively regulate their RTP. According to this consideration, several carbonyl-based small organic molecules (Fig. 1), including aliphatic heterocyclic and linear molecules, are introduced into the matrix of polysiloxanes as guests. They are maleimide (MI), maleic anhydride (MA), succinic anhydride (SA), acrylamide (AM), oxalamide (OM) and malonamide (MN). A series of doped polysiloxane nanocomposites (PAS-MA, PAS-MN, PAS-OM, PAM-SA, PAM-MI, PAS-AM and PUS-MI) can be obtained, following the synthetic route in Scheme S2.† Guest molecules were expected to form clusters with functional groups of polysiloxane. Due to the fixation of the clusters, and the package of the silicone framework, the guest molecules would not be filtered out. The crystalline structure of the composites was characterized by PXRD (Fig. S11†). PXRD patterns of all nanocomposites only show the characteristic peak of silica at 23°, which indicates that the doping of the organic guest did not affect the amorphous structure of the polysiloxane matrix.

Fig. 5a shows the luminescence photographs of the nanocomposites when the UV lamp is turned on and off. Their afterglow color covers the entire visible light region from blue to red. Fig. 5b and c show the prompt and delayed photoluminescence spectra of the nanocomposites, respectively.
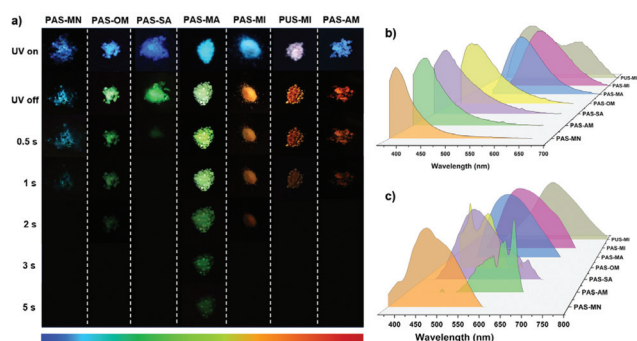
Their delayed emission wavelengths range from 380 nm to 638 nm. Consequently, full-color afterglow of polysiloxanes has been achieved by changing the type of guest molecule. The guests (MA, MI, and AM) containing C= double bonds lead to the obvious red shift of the phosphorescence emission wavelength of the nanocomposites. For instance, the delayed emission peak of PAS-MA locates at 530 nm which is 32 nm longer than that of PAS-SA (at 498 nm). The luminescence quantum yields were measured and are summarized in Table 1, while the RTP lifetimes of these polysiloxane nanocomposites were obtained from their time-resolved luminescence decay curves (Fig. S12 and Table S4†). Among them, PAS-MN exhibits the highest photoluminescence quantum yield (Φ = 44%). This can be attributed to the unique structure of MN, two amide groups and one methylene group, which endows it with a strong ability to form intermolecular forces within clusters. As a result, the clusters formed in PAS-MN are very rigid, which improves the radiation decay of excitons. However, its lifetimes of RTP at 450 nm is not long (τ = 132 ms); thus the blue afterglow only lasts for 1s. Notably, PAS-MA shows the longest RTP lifetime of 576 ms at 530 nm with a relatively high quantum yield of 30.4%, which make its green afterglow last for 5 s. The afterglow time is 10 times longer than that of PAS-SA with a similar guest to PAS-MA. In addition, PUS-MI exhibits a unique white emission under UV irradiation with a CIE of (0.30, 0.30), which is attributed to a dual emission: orange-red phosphorescence at 585 nm and blue fluorescence at 472 nm (Fig. S13†).

Then, the content of MI was changed to regulate the luminescence properties of PAS-MI composites. By fixing the ratio of AS and MI to 5 : 1, 1 : 1, and 1 : 5, the effect of MI doping content on the RTP of PAS-MI was investigated. Their FT-IR spectra (Fig. S14†) show that the carbonyl characteristic peak at about 1700 cm^{-1} becomes stronger with the increase of the MI doping ratio, while the characteristic peak of NH$_2$ decreases gradually. Fig. 6a shows the photographs of PAS-MI composites with different doping ratios under daylight and UV light. With the increasing ratio of AS to MI, the color of composites turns from white to light-yellow, and then to red, while the emission color is adjusted from blue to blue-green, and

Fig. 5 (a) Photographs of the nanocomposites before and after UV light is turned off. Prompt (b) and delayed (c) photoluminescence spectra of the nanocomposites (t_d = 1 ms).

Table 1 Photophysical properties of the nanocomposites

	Fluorescence		Phosphorescence		
Sample	λ_{ex} (nm)	λ_{em} (nm)	λ_{em} (nm)	τ (ms)	Φ^a
PAS-MN	338	373	380	67.6	44
			450	132.7	
AS-OM	342	407	451	262.8	9.16
			501	252.7	
PAS-SA	335	390	498	49.5	14.1
PAS-MA	400	495	530	576.2	30.4
PAS-MI	410	507	550	254.5	16
PAS-AM	331	390	584	93	12.6
			638	80	
PUS-MI	370	472	620	322.4	2.88

^{a} Total luminescence quantum yield.

3622 | *Inorg. Chem. Front.*, 2022, **9**, 3619–3626

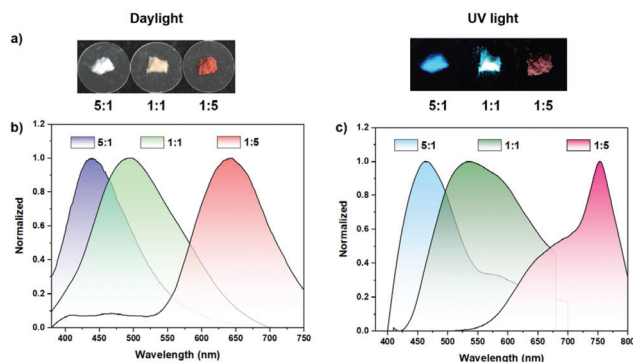This journal is © the Partner Organisations 2022

Fig. 6 (a) Photographs of PAS-MI composites with different ratios of AS and MI under daylight and UV light. Prompt (b) and delayed (c) photoluminescence spectra of PAS-MI with the different ratios of AS and MI.

then to dark-red. The maximum emission peaks of the prompt and delayed emission spectra of the composites are gradually red-shifted from the blue to red region with the increase of MI contents (Fig. 6b). Notably, PAS-MI exhibits near-infrared phosphorescence emission (λ_{em} = 753 nm) with a phosphorescence lifetime of 0.163 ms when the ratio of AS to MI reaches 1 : 5 (Fig. 6c). Their specific photophysical data are listed in Table S5.†

The experimental results show that there is a synergistic effect between the organic guest and siloxane in polysiloxane nanocomposites, and that the guest with different doping ratios can form different kinds of clusters with siloxane. When the content of MI is much smaller than that of AS, the space cluster mainly relies on the hydrogen bonding between the amino group and the uncross-linked silanol, and a small portion of MI is involved in the overall cluster formation (Fig. S15†). Consequently, PAS-MI with a 5 : 1 molar ratio of AS and MI shows similar luminescence properties to PAS (Fig. S16†). As the content of MI increases, it can be expected that the interaction between organic molecules and siloxane functional groups becomes stronger and stronger. When the molar ratio of AS and MI is at 1 : 1, the host–guest can form stable spatial clusters, thus resulting in the strong emission. If the content of MI continues to increase, MI will gradually replace AS as the main body of the composite. The double bonds of multiple MI molecules are combined to form a larger π–π spatial conjugate system, which causes a red shift of prompt and delayed emissions. As a result, PAS-MI with a 1 : 5 molar ratio of AS and MI shows near-infrared RTP. However, because MI becomes the main body of the composite, the fixation effect of the silica skeleton becomes weak, which leads to non-radiative deactivation and a significant decrease in luminescence efficiency.

Metal ion detection

Silver ions are widely used in sterilization,[31] medical treatment[32] and cosmetics,[33] but they can inactivate some biological enzymes in the body.[34,35] When the content of Ag$^+$ in the body exceeds the critical concentration, it will also cause

certain harm to the liver.[36] Therefore, the detection of Ag$^+$ is very important. However, the current detection methods of Ag$^+$, mainly including atomic absorption spectrometry, atomic emission spectrometry, inductively coupled plasma mass spectrometry and so on, need complex procedures and expensive experimental equipment.[37,38] An optical method based on luminescent probes with rapid responses, low cost, and flexibility, is valuable and convenient for Ag$^+$ detection. It is very necessary to develop a fast, accurate and efficient Ag$^+$ luminescent probe, especially a phosphorescent one with high sensitivity. The PAS nanomaterial was selected as the probe to detect Ag$^+$ in aqueous solutions. A variety of different metal ions (Cu$^+$, Cu^{2+}, Mg^{2+}, Na$^+$, Al^{3+}, In^{3+}, Pb^{2+}, Hg^{2+}, Ni^{2+}, Cd^{2+}, and Fe^{3+}) were configured into 0.2 mM aqueous solutions, and then 2 mg of PAS powders were added into 2 ml of the metal ion solution, and soaked for 1 min. Considering the effect of water on the cluster luminescence, PAS was filtered and dried at 100 °C for 1 min before the detection. Fig. S17a† shows the photographs of PAS treated with different ionic solutions before and after turning off the UV lamp. Among these ions, Ag$^+$ imposes an excellent quenching effect on both the fluorescence and phosphorescence of PAS (Fig. S17b and S17c†). In particular, the phosphorescence intensity of PAS is quenched by 97% with Ag$^+$ aqueous solution (Fig. 7a).

To establish the working curve of Ag$^+$ quantitative detection, the effect of Ag$^+$ concentration on the luminescence performance of PAS was investigated in aqueous solution (Fig. 7b–d). The prompt and delayed emission intensity of PAS shows an excellent linear response with increasing Ag$^+$ concentration (prompt: $y = -0.037 \ln(c) + 0.2044$, $R^2 = 0.9933$; delay $y = -0.048 \ln(c) + 0.0889$, $R^2 = 0.9830$). The Ag$^+$ detection limit for the steady-state luminescence intensity of PAS was 0.027
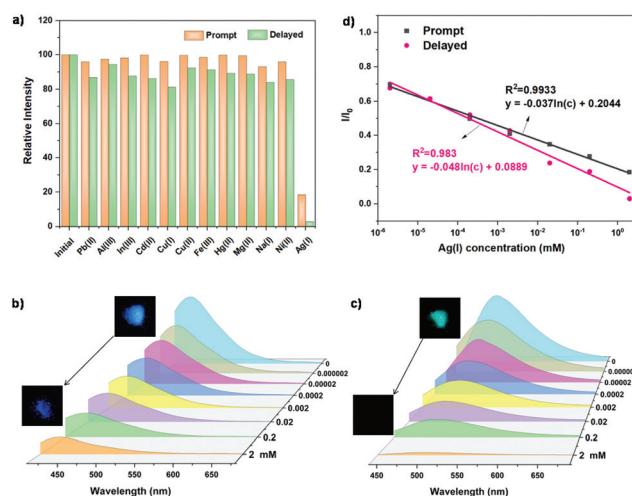

Fig. 7 (a) Relative intensity of prompt and delayed emission of PAS in the presence of different metal ions (2 mM). Prompt (b) and delayed (c) photoluminescence spectra of PAS after immersion in Ag$^+$ solutions of different concentrations (λ_{ex} = 365 nm). (d) The linear correlation between PAS prompt and delayed emission relative intensity and Ag$^+$ concentration.

This journal is © the Partner Organisations 2022

Inorg. Chem. Front., 2022, **9**, 3619–3626 | **3623**

nM, which is very close to the lowest detection limit of the reported Ag$^+$ probes (Table S1†). As mentioned above, PAS luminescence is due to the formation of specific clusters. Metal ions maybe destroy the formation of clusters by coordinating with N atoms, resulting in the quenching of cluster luminescence.[39] Among these detected metal ions, Ag$^+$ has the smallest charge/radius ratio (Table S6†). The smaller the charge/radius ratio of the metal, the stronger the metallicity, and the easier it is to combine with the amino group of PAS to form a complex. Consequently, Ag$^+$ ions lead to the collapse of spatial clusters and luminescence quenching of PAS.

In order to verify the detection mechanism of Ag$^+$, PAS and treated PAS with Ag$^+$ ions were analysed by *in situ* attenuated total reflection (ATR) IR and solid-state NMR. As shown in the ATR-IR spectra (Fig. S18†), the addition of Ag$^+$ ions caused the –NH$_2$ stretching vibration peak originally located at 3300 cm^{-1} to move significantly to the direction of a low wavenumber. This shows that Ag$^+$ ions can interact with the amine groups of PAS and destroy the cluster structure. However, when Cu$^+$ and Na$^+$ ions are added to PAS, the amine stretching vibration peak of PAS hardly changes. The solid-state NMR spectrum of PAS shows that there is only a wide signal peak at 2.34 ppm (Fig. S19†). The hydrogen of amino and methylene was fixed and ossified by the cluster structure, thus showing a wide NMR peak. However, when PAS interacts with Ag$^+$ ions, Ag$^+$ ions would quickly complex with the amino group, resulting in cluster collapse. Consequently, the NMR signal of methylene connected to the amino group clearly appears at 2.69 ppm. These results confirm the detection mechanism of PAS for Ag$^+$ ions, that is, the luminescence quenching caused by cluster collapse. To recycle PAS, the Ag$^+$-treated powder was washed with water three times. Interestingly, because the Ag$^+$ ions were removed by water, the clusters based on –NH$_2$ terminal groups were regenerated, resulting in the recovery of the fluorescence and phosphorescence of PAS (Fig. S20a†). After ten times recycling of detection/washing, the PAS probe still maintained a highly sensitive response to Ag$^+$ ions (Fig. S20b and S20c†).

In practical application, the composition of environmental water samples is often very complex. There are not only soluble heavy metal ions, but also other impurities including some soluble dyes, such as rhodamines and its derivatives. These fluorescent dyes have a very serious background interference to the Ag$^+$ detection of traditional fluorescent probes. The PAS probe has fluorescence/phosphorescence double responses to Ag$^+$, and in particular the phosphorescence detection can avoid the interference of the fluorescence background. Moreover, the double response can also verify the accuracy of the detection results, avoid multiple tests on the same sample, and greatly improve the detection efficiency and accuracy. The above standard curves were used to detect the concentration of Ag$^+$ in city water and commercial silver ion bacteriostatic agents, to explore the reliability of the PAS probe in practical applications. Prompt and delayed emission spectra of the PAS probe treated with the two aqueous samples are shown in Fig. 8a. City water causes a small decrease in the prompt and delayed emission intensity of PAS, while bacteriostatic agents lead to a significant decrease (Fig. 8b). According to the prompt and delayed emission intensity, the concentration of Ag$^+$ was calculated from the standard working curves to be 8.964 pM and 8.955 pM, respectively. Their average value (8.96 pM) meets the national standard of Ag$^+$ concentration in drinking water (<0.46 μM). For a bacteriostatic sample, the average value of Ag$^+$ concentration was calculated to be 2.48 mM, which is consistent with the data (2.24–2.60 mM) provided by the manufacturer (Fig. 8c).

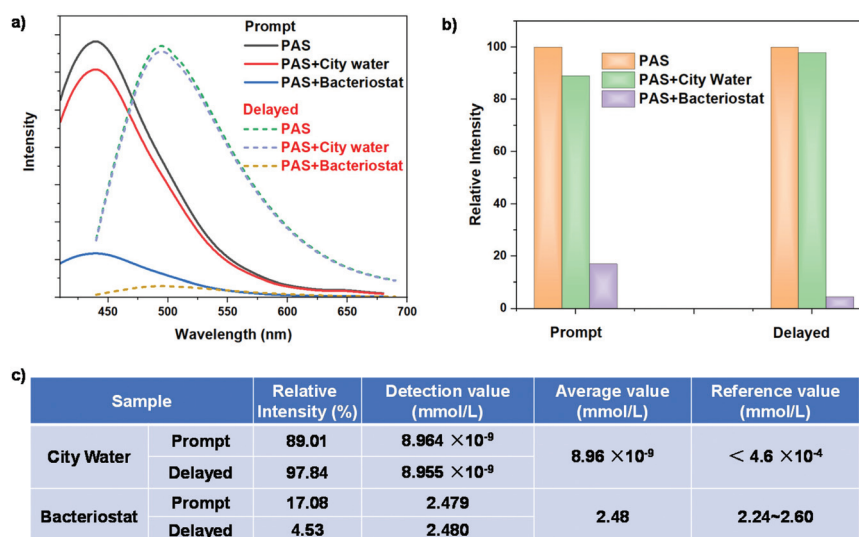| Sample		Relative Intensity (%)	Detection value (mmol/L)	Average value (mmol/L)	Reference value (mmol/L)
City Water	Prompt	89.01	8.964 ×10^{-9}	8.96 ×10^{-9}	< 4.6 ×10^{-4}
	Delayed	97.84	8.955 ×10^{-9}		
Bacteriostat	Prompt	17.08	2.479	2.48	2.24~2.60
	Delayed	4.53	2.480		

Fig. 8 Prompt and delayed emission spectra (a) and relative intensity (b) of PAS treated with different water samples. (c) Detection and standard reference values of Ag$^+$ concentration for city water and bacteriostatic agent.

3624 | *Inorg. Chem. Front.*, 2022, **9**, 3619–3626

This journal is © the Partner Organisations 2022

Conclusions

A series of crosslinked polysiloxane nanomaterials with different terminal groups were synthesized by the solution method. The polysiloxanes with amino (PAS) and urea (PUS) groups show high quantum yield and long-lived RTP for the formation of luminescent clusters. Their prompt and delayed emissions show excitation wavelength-dependent properties because the different sizes of clusters produce multiple luminescent centers. Using the skeletons of PAS and PUS as the host, the full-color afterglow with high quantum yield (up to 44%), long lifetime (up to 560 ms), and adjustable emissive wavelength (380–753 nm) has been achieved by doping different types and contents of organic guest small molecules. The rapid, efficient and accurate detection of Ag^+ in aqueous solution was realized by using the amino group of PAS. With the increase of Ag^+ concentration, the prompt and delayed emission intensity of PAS decreased linearly with a detection limit as low as 0.027 nM, which has a higher sensitivity compared with other Ag^+ probes. Through the detection of Ag^+ concentration in city water and commercial silver ion bacteriostatic agents, the double response of the PAS probe for silver ions is highly reliable and has good application prospects. The works provide a new idea to regulate the long-lived RTP of cluster-luminescent nanomaterials and display a huge potential in the fields of ion sensing.

Author contributions

Zhenghuan Lin: conceptualization, project administration, supervision, and writing – review & editing. Shuaiqi Wang: formal analysis, investigation, methodology, validation, visualization, and writing – original draft. Xiaolang Wang: investigation and methodology. Shangwei Feng: data curation. Wei Lv: detection of metal ions. Meijuan Lin: editing. Qidan Ling: resources.

Conflicts of interest

There are no conflicts to declare.

Acknowledgements

Notes and references

1 Q. Peng, H. Ma and Z. Shuai, Theory of Long-Lived Room-Temperature Phosphorescence in Organic Aggregates, *Acc. Chem. Res.*, 2021, **54**, 940–949.

2 S. Guo, W. Dai, X. Chen, Y. Lei, J. Shi, B. Tong, Z. Cai and Y. Dong, Recent Progress in Pure Organic Room Temperature Phosphorescence of Small Molecular Host–Guest Systems, *ACS Mater. Lett.*, 2021, **3**, 379–397.

3 J. Wang, Z. Liu, S. Yang, Y. Lin, Z. Lin and Q. Ling, Large Changes in Fluorescent Color and Intensity of Symmetrically Substituted Arylmaleimides Caused by Subtle Structure Modifications, *Chem. – Eur. J.*, 2018, **24**, 322–326.

4 B. Chen, W. Huang, X. Nie, F. Liao, H. Miao, X. Zhang and G. Zhang, An Organic Host-Guest System Producing Room-Temperature Phosphorescence at the Parts-Per-Billion Level, *Angew. Chem., Int. Ed.*, 2021, **60**, 16970–16973.

5 A. D. Nidhankar, Goudappagouda, V. C. Wakchaure and S. S. Babu, Efficient metal-free organic room temperature phosphors, *Chem. Sci.*, 2021, **12**, 4216–4236.

6 D. Wu, W. Gong, H. Yao, L. Huang, Z. Lin and Q. Ling, Highly efficient solid-state emission of diphenylfumaronitriles with full-color AIE, and application in explosive sensing, data storage and WLEDs, *Dyes Pigm.*, 2020, **172**, 107829.

7 G. Tang, K. Zhang, T. Feng, S. Tao, M. Han, R. Li, C. Wang, Y. Wang and B. Yang, One-step preparation of silica microspheres with super-stable ultralong room temperature phosphorescence, *J. Mater. Chem. C*, 2019, **7**, 8680–8687.

8 J. Deng, H. Wu, W. Xie, H. Jia, Z. Xia and H. Wang, Metal Cation-Responsive and Excitation-Dependent Nontraditional Multicolor Fluorescent Hydrogels for Multidimensional Information Encryption, *ACS Appl. Mater. Interfaces*, 2021, **13**, 39967–39975.

9 X. Dou, T. Zhu, Z. Wang, W. Sun, Y. Lai, K. Sui, Y. Tan, Y. Zhang and W. Z. Yuan, Color-Tunable, Excitation-Dependent, and Time-Dependent Afterglows from Pure Organic Amorphous Polymers, *Adv. Mater.*, 2020, **32**, e2004768.

10 S. Y. Lin, T. H. Wu, Y. C. Jao, C. P. Liu, H. Y. Lin, L. W. Lo and C. S. Yang, Unraveling the photoluminescence puzzle of PAMAM dendrimers, *Chem. – Eur. J.*, 2011, **17**, 7158–7161.

11 H. Wang, Q. Lu, M. Li, H. Li, Y. Liu, H. Li, Y. Zhang and S. Yao, Electrochemically prepared oxygen and sulfur co-doped graphitic carbon nitride quantum dots for fluorescence determination of copper and silver ions and biothiols, *Anal. Chim. Acta*, 2018, **1027**, 121–129.

12 R. B. Restani, P. I. Morgado, M. P. Ribeiro, I. J. Correia, A. Aguiar-Ricardo and V. D. Bonifacio, Biocompatible polyurea dendrimers with pH-dependent fluorescence, *Angew. Chem., Int. Ed.*, 2012, **51**, 5162–5165.

13 Q. Zhou, Z. Wang, X. Dou, Y. Wang, S. Liu, Y. Zhang and W. Z. Yuan, Emission mechanism understanding and tunable persistent room temperature phosphorescence of amorphous nonaromatic polymers, *Mater. Chem. Front.*, 2019, **3**, 257–264.

14 J. Li, P. Shen, Z. Zhao and B. Z. Tang, Through-Space Conjugation: A Thriving Alternative for Optoelectronic Materials, *CCS Chem.*, 2019, **1**, 181–196.

15 H. Zhang and B. Z. Tang, Through-Space Interactions in Clusteroluminescence, *JACS Au*, 2021, **1**, 1805–1814.

16 S. Tang, T. Yang, Z. Zhao, T. Zhu, Q. Zhang, W. Hou and W. Z. Yuan, Nonconventional luminophores: characteristics, advancements and perspectives, *Chem. Soc. Rev.*, 2021, **50**, 12616–12655.

17 G. Farias, C. A. M. Salla, M. Aydemir, L. Sturm, P. Dechambenoit, F. Durola, B. de Souza, H. Bock, A. P. Monkman and I. H. Bechtold, Halogenation of a twisted non-polar pi-system as a tool to modulate phosphorescence at room temperature, *Chem. Sci.*, 2021, **12**, 15116–15127.

18 H. Sun, R. Ding, S. Lv, S. Zhou, S. Guo, Z. Qian and H. Feng, Clustering-Triggered Ultralong Room-Temperature Phosphorescence of Organic Crystals through Halogen-Mediated Molecular Assembly, *J. Phys. Chem. Lett.*, 2020, **11**, 4962–4969.

19 X. Zheng, Y. Huang, D. Xiao, S. Yang, Z. Lin and Q. Ling, Space conjugation induced white light and room-temperature phosphorescence from simple organic small molecules: single-component WLED driven by both UV and blue chips, *Mater. Chem. Front.*, 2021, **5**, 6960–6968.

20 Y. Zheng, Z. Wang, J. Liu, Y. Zhang, L. Gao, C. Wang, X. Zheng, Q. Zhou, Y. Yang, Y. Li, H. Tang, L. Qu, Y. Zhao and C. Yang, Long-Lived Room Temperature Phosphorescence Crystals with Green Light Excitation, *ACS Appl. Mater. Interfaces*, 2022, **14**, 15706–15715.

21 P. Liao, S. Zang, T. Wu, H. Jin, W. Wang, J. Huang, B. Z. Tang and Y. Yan, Generating circularly polarized luminescence from clusterization-triggered emission using solid phase molecular self-assembly, *Nat. Commun.*, 2021, **12**, 5496.

22 S. Wang, J. Wang, Q. Huang, X. Zheng, Z. Yao, S. Xiang, Q. Ling and Z. Lin, Greatness in Simplicity: Efficient Red Room-Temperature Phosphorescence from Simple Halogenated Maleimides with a 2D Layered Structure, *ACS Appl. Mater. Interfaces*, 2022, **14**, 14703–14711.

23 T. Zhu, T. Yang, Q. Zhang and W. Z. Yuan, Clustering and halogen effects enabled red/near-infrared room temperature phosphorescence from aliphatic cyclic imides, *Nat. Commun.*, 2022, **13**, 2658.

24 S. Wang, D. Wu, S. Yang, Z. Lin and Q. Ling, Regulation of clusterization-triggered phosphorescence from a non-conjugated amorphous polymer: a platform for colorful afterglow, *Mater. Chem. Front.*, 2020, **4**, 1198–1205.

25 J. Guo, C. Yang and Y. Zhao, Long-Lived Organic Room-Temperature Phosphorescence from Amorphous Polymer Systems, *Acc. Chem. Res.*, 2022, **55**, 1160–1170.

26 M. Cui, M. Li, J. Wang, R. Chen, Z. Xu, J. Wang, J. Han, G. Hu, R. Sun, X. Jiang, B. Song and Y. He, Hydrothermal Synthesis of Zinc-Doped Silica Nanospheres Simultaneously Featuring Stable Fluorescence and Long-Lived Room-Temperature Phosphorescence, *Angew. Chem., Int. Ed.*, 2021, **60**, 15490–15496.

27 H. Lu, L. Feng, S. Li, J. Zhang, H. Lu and S. Feng, Unexpected Strong Blue Photoluminescence Produced from the Aggregation of Unconventional Chromophores in Novel Siloxane–Poly(amidoamine) Dendrimers, *Macromolecules*, 2015, **48**, 476–482.

28 Y. Feng, T. Bai, H. Yan, F. Ding, L. Bai and W. Feng, High Fluorescence Quantum Yield Based on the Through-Space Conjugation of Hyperbranched Polysiloxane, *Macromolecules*, 2019, **52**, 3075–3082.

29 Q. Huang, H. Gao, S. Yang, D. Ding, Z. Lin and Q. Ling, Ultrastable and colorful afterglow from organic luminophores in amorphous nanocomposites: advanced anti-counterfeiting and in vivo imaging application, *Nano Res.*, 2020, **13**, 1035–1043.

30 J. H. Kim, K. B. Kim, J. S. Park and N. Min, Single cytosine-based electrochemical biosensor for low-cost detection of silver ions, *Sens. Actuators, B*, 2017, **245**, 741–746.

31 L. Xu, X. Shi, Q. Qian, X. Bai, L. Xu and Q. Wang, Hydrothermal sterilization in silver nitrate solution endows plasma sprayed hydroxyapatite coating with antibacterial property, *Mater. Lett.*, 2020, **263**, 127258.

32 X. X. Liang, S. X. Luan, Z. Q. Yin, M. He, C. L. He, L. Z. Yin, Y. F. Zou, Z. X. Yuan, L. X. Li, X. Song, C. Lv and W. Zhang, Recent advances in the medical use of silver complex, *Eur. J. Med. Chem.*, 2018, **157**, 62–80.

33 L. Salvioni, E. Galbiati, V. Collico, G. Alessio, S. Avvakumova, F. Corsi, P. Tortora, D. Prosperi and M. Colombo, Negatively charged silver nanoparticles with potent antibacterial activity and reduced toxicity for pharmaceutical preparations, *Int. J. Nanomed.*, 2017, **12**, 2517–2530.

34 W. Zhang, Y. Luo, Y. Zhou, M. Liu, W. Xu, B. Bian, Z. Tao and X. Xiao, A highly selective fluorescent chemosensor probe for detection of Fe^{3+} and Ag^+ based on supramolecular assembly of cucurbit[10]uril with a pyrene derivative, *Dyes Pigm.*, 2020, **176**, 108235.

35 Y. Zhang, W. Chen, X. Dong, H. Fan, X. Wang and L. Bian, Simultaneous detection of trace toxic metal ions, Pb^{2+} and Ag^+, in water and food using a novel single-labeled fluorescent oligonucleotide probe, *Sens. Actuators, B*, 2018, **261**, 58–65.

36 J. Poznanski, D. Soldacki, B. D. Czarkowska-Paczek, A. Bonna, O. Kornasiewicz, M. Krawczyk, W. Bal and L. Paczek, Cirrhotic Liver of Liver Transplant Recipients Accumulate Silver and Co-Accumulate Copper, *Int. J. Mol. Sci.*, 2021, **22**, 1782.

37 Q. W. He, E. W. Miller, A. P. Wong and C. J. Chang, A selective fluorescent sensor for detecting lead in living cells, *J. Am. Chem. Soc.*, 2006, **128**, 9316–9317.

38 M. Li, H. Gou, I. Al-Ogaidi and N. Wu, Nanostructured Sensors for Detection of Heavy Metals: A Review, *ACS Sustainable Chem. Eng.*, 2013, **1**, 713–723.

39 Z. Zhou, Y. Ding, S. Si, W. Wu, C. Deng, H. Wu and J. Xiang, Wide-field determination of aqueous mercury(II) based on tail-extensible DNA fluorescent probe with tunable dynamic range, *J. Hazard. Mater.*, 2021, **417**, 125975.